Chemical Science

ROYAL SOCIETY OF CHEMISTRY

EDGE ARTICLE

View Article Online
View Journal | View Issue

Cite this: *Chem. Sci.*, 2020, **11**, 6305

All publication charges for this article have been paid for by the Royal Society of Chemistry

Received 26th March 2020
Accepted 27th May 2020

DOI: 10.1039/d0sc01762k

rsc.li/chemical-science

Enhanced proton conductivity in a layered coordination polymer†

Ricardo F. Mendes, ‡*[a] Paula Barbosa, ‡[b] Eddy M. Domingues, [b] Patrícia Silva,[a] Filipe Figueiredo *[b] and Filipe A. Almeida Paz *[a]

$[Gd(H_4nmp)(H_2O)_2]Cl\cdot 2H_2O$ (**1**) converts into $[Gd_2(H_3nmp)_2]\cdot xH_2O$ (**2**) ($x = 1$ to 4) with a notable increase in proton conductivity. **1** is a charged layered material counter balanced by chloride ions, with proton conductivity values of 1.23×10^{-5} S cm^{-1} at 98% relative humidity (RH) and 40 °C. At 98% RH and 94 °C the observed conductivity is 0.51 S cm^{-1}, being to date one of the highest values ever reported for a proton-conducting coordination polymer. This increase is observed during a structural transformation into **2** that occurs at high temperature and RH. While this remarkable conductivity is observed only after transformation and by maintaining high humidity conditions, as-synthesized **2** also shows a conductivity value of 3.79×10^{-2} S cm^{-1} at 94 °C and 98% RH, still ranked as one of the highest reported values. Moreover, it is shown that the key factor for high proton conduction is the unusual dynamic structural transformation with water insertion and release of chloride ions.

Introduction

Advances in the area of materials chemistry often require understanding on how physico-chemical properties may influence a targeted application. Metal–Organic Frameworks (MOFs) and Coordination Polymers (CPs) are crystalline compounds that advantageously allow, to a point, the design and construction of different architectures envisaging a desired applicability.[1,2] It is, thus, not surprising that these materials have been investigated for broad areas, ranging from storage/incorporation of gases and molecules,[3] to catalysis,[4,5] photoluminescence,[6,7] and drug delivery,[8,9] among many others that are important to society.[10–12]

An important area that has gained increased interest is that of fuel cells, more precisely, the development of materials with improved proton conduction.[13–17] MOFs and CPs can be designed with different types of pores or channels which are normally filled with proton conducting species, such as water or charged species. Not only that, but these materials can also bear organic linkers rich in protons (*e.g.*, phosphonic or sulfonic acid groups). They are expected, *a priori*, to boost proton conductivity. The rising energy consumption is, thus, a current and pertinent driving force to search for alternative energy technologies. This remarkable ability of MOFs/CPs to be tailored to better conduct protons can make them ideal candidates to be incorporated, for example, into composite membranes and films for fuel cells.[18] For example, highly proton conductive MOFs or CPs can be designed by increasing the concentration of dissociated proton carriers (*e.g.*, by the inclusion of acidic species), and by tailoring host scaffolds that allow hydrogen bonding interactions as efficient proton-conducting pathways inside pores and channels.[13]

Phosphonate-based MOFs have attracted the attention of the research community mostly due to increased chemical and thermal stabilities when compared to carboxylate-based MOFs and also the acidity of the many P–OH groups present in the final materials.[19–22] This, allied to the ability to determine, with precision, the features of CPs and MOFs by X-ray diffraction, opens the possibility of structurally visualizing potential ion transfer pathways. High-dimensional networks with 1D or 2D channels filled with solvent molecules (particularly water) and with non-coordinated –POH groups may, thus, suggest the possibility of proton conductivity.

In this report we explore how subtle structural changes between two related layered CPs can lead to a remarkable enhancement in proton conductivity: $[Gd(H_4nmp)(H_2O)_2]Cl\cdot 2H_2O$ (**1**) (previously reported by us)[4] converts *in situ*, at high humidity and temperatures, into $[Gd_2(H_3nmp)_2]\cdot xH_2O$ (**2**) ($x =$ 1 to 4 water molecules; H_6nmp stands for nitrilotris(methylenephosphonic)acid), which is shown to be a hydrophilic compound with variable interlayer space. The observed proton conductivities for the latter compound (which can also be directly isolated from typical and sustainable syntheses) are, to the best of our knowledge, some of the best reported

[a]*Department of Chemistry, CICECO – Aveiro Institute of Materials, University of Aveiro, 3810-193 Aveiro, Portugal. E-mail: filipe.paz@ua.pt*

[b]*Department of Materials & Ceramic Engineering, CICECO – Aveiro Institute of Materials, University of Aveiro, 3810-193 Aveiro, Portugal*

† Electronic supplementary information (ESI) available. CCDC 1960178. For ESI and crystallographic data in CIF or other electronic format see DOI: 10.1039/d0sc01762k

‡ The authors contributed equally to the work.

conductivities to date, even surpassing those of commercial materials.

Results and discussion

Synthesis and initial structural assessment

The presence of phosphonate-containing ligands with hydrogen-bonded chains in $[Gd(H_4nmp)(H_2O)_2]Cl\cdot 2H_2O$ (**1**) makes it a suitable host to enable ionic transport along the interlayer space, where the adsorption of water molecules can strongly be facilitated by the phosphonic acid groups, thus forming pathways for the structural diffusion of protons. **1** has 2D charged layers, counter-balanced by chloride anions located in the interlayer spaces. –POH groups and coordinated water molecules of the $^{2}_{\infty}[Gd(H_4nmp)(H_2O)_2]^{+}$ cationic layer donate their hydrogen atoms to neighbouring water molecules of crystallization and to chloride anions. The conductivity of **1** at variable temperatures (40 and 60 °C) and relative humidity (RH, 20–98%) previously reported by us[4] reached 1.23×10^{-5} S cm^{-1} at 40 °C and 98% RH, which compares favourably with those of other CPs/MOFs reported in the literature.[13]

In our studies throughout the years on the usage of H_6nmp and lanthanide cations, the new phase herein formulated as $[Gd_2(H_3nmp)_2]\cdot xH_2O$ (**2**) (x = 1 to 4) was periodically isolated under different synthetic conditions and with distinct morphologies. We also note that Bazaga-García isolated this material after conductivity studies, reporting solely a simple diffractogram with no extra characterisation.[19] The "apparent" poor quality of these powder X-ray diffractograms is attributed

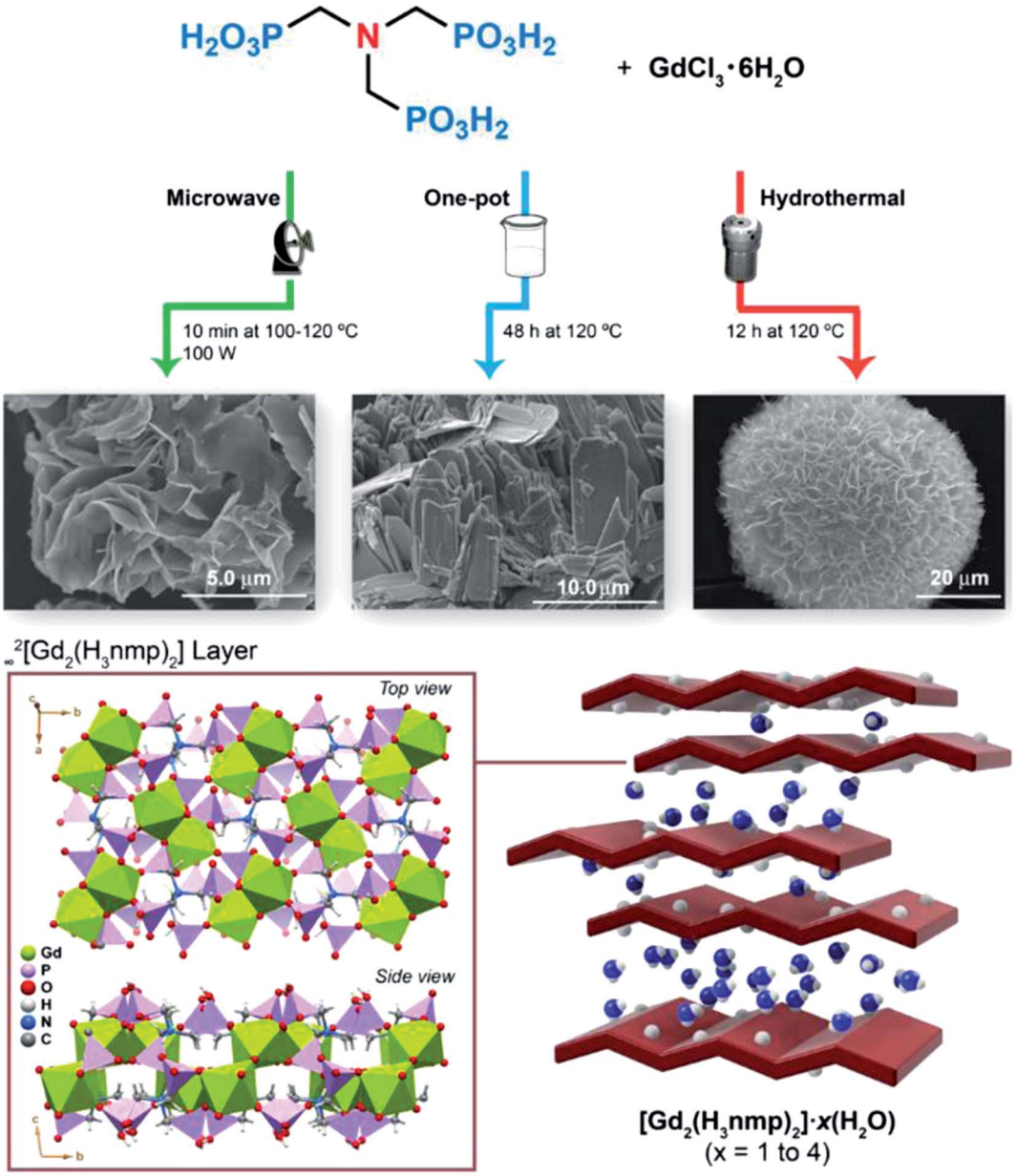

Fig. 1 Schematic representation of the synthesis and structural features of $[Gd_2(H_3nmp)_2]\cdot xH_2O$ (**2**, with x = 1 to 4).

to "poor" crystallinity of the product. However, following our previous work on **1**,[4] the observed *in situ* structural transformation at high temperatures and RH (above 80 °C and at 98% RH) of **1** into **2**, and the remarkable properties of the latter, prompted us to reinvestigate in more detail the structural features of this new compound.

We stress that **2** could be directly isolated using three distinct approaches (Fig. 1): conventional hydrothermal, microwave-assisted and one-pot conditions, typically as thin plate-like crystals (further details concerning synthesis optimization, crystal morphology and crystal structure description of **2** are provided in the ESI†). We further note that both **1** and **2** can be easily and readily prepared in a rapid, cost-effective and environmentally safe (and conscious) manner. It is noteworthy that microwaves allow the isolation of both compounds in only a few minutes (20 min for **1** and just 10 min for **2**) using water as the sole solvent. We note that despite using different methods for the preparation of **1** and **2**, the same crystalline phase was obtained, as observed by powder X-ray diffraction analysis (Fig. S1†).

Structural transformation

$[Gd_2(H_3nmp)_2]\cdot xH_2O$ (**2**) (x = 1 to 4) could be obtained under two very distinct conditions: directly from any synthesis used (see the Experimental section in the ESI† and Fig. 1) or, unexpectedly, from *in situ* conversion of $[Gd(H_4nmp)(H_2O)_2]Cl\cdot 2H_2O$ (**1**) above a certain temperature and RH. The crystal structure of **2** eluded us for almost a decade; powder X-ray diffraction patterns could not be indexed (even those collected at various synchrotron sources), and crystals were simply not large enough to be collected using single-crystal X-ray diffraction (again, even using various beam lines at synchrotron sources). A poor crystalline aggregate was serendipitously isolated from hundreds of trial-and-error syntheses using the one-pot method, which permitted the derivation of a structural model for **2**; $[Gd_2(H_3nmp)_2]\cdot 1.4H_2O$ (**2sc**) was refined with all the structural details being given in the ESI.† **2sc** was found to crystallize in the triclinic $P\bar{1}$ space group sharing some structural features with **1** but having instead solely water molecules in the interstitial space (see the ESI† for further details and Fig. 1). We stress that this structural model could not exactly fit any experimental powder X-ray diffraction pattern collected over the many years of preparation of **2**. This fact was always allied with other, sometimes contradicting, features:

(a) the amount of water derived from TG analysis was typically higher for **2** than **2sc**;

(b) solid-state NMR data of various compounds always fitted the requirement of just four equally abundant phosphorus sites in the asymmetric unit;

(c) the overlap of laboratory powder X-ray diffraction patterns showed a distribution of the first more intense reflection over a 2 theta range greater than 0.5°, which cannot simply be attributed to either zero shift or other instrumental corrections (Fig. S2 in the ESI†).

Thus, and considering the features observed during the proton conductivity measurements, we believe that **2** has a variable interlayer space with a distinct number of water molecules (hydrogen-bonded to the neutral layers and to each other). This clearly explains the statistical distribution of water molecules for the various isolated compounds and the variable position of the (002) reflection in the powder patterns. Though the layers are "disordered" in the *ab* plane with a variable *c*-axis length, the local environments of the phosphorous sites remain unchanged, hence the four observed sites.

The transformation of **1** into **2** is believed to be induced, at first, by the inclusion of a large number of water molecules in the interstitial space (Fig. 2). This flow of water "swells" the material, separating the layers farther from each other, thus weakening most of the hydrogen bonding interactions. At this stage the exchange of the chloride ions for water occurs, with one of the protons from the 2D layer being removed alongside the Cl^- anion, rendering the aforementioned layers neutral and

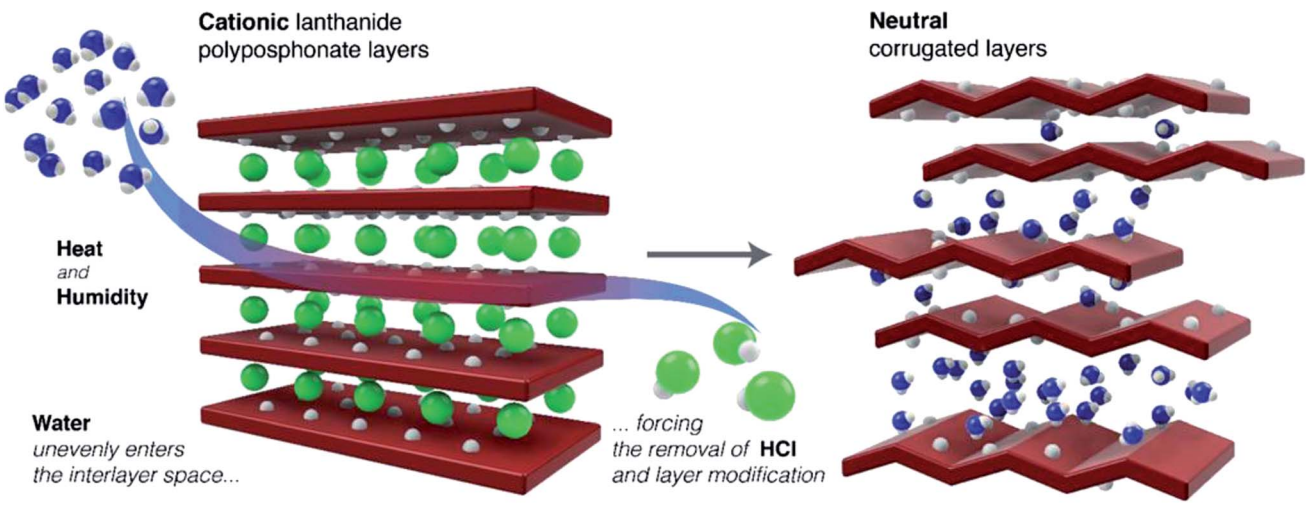

Fig. 2 Schematic representation of the structural transformation of $[Gd(H_4nmp)(H_2O)_2]Cl\cdot 2H_2O$ (**1**, left) into $[Gd_2(H_3nmp)_2]\cdot xH_2O$ (**2**, right) (x = 1 to 4) at high temperatures and humidity. The figure emphasizes the release of the Cl^- anion as hydrochloric acid and the irregular rearrangements of the $^2_\infty[Gd_2(H_3nmp)_2]$ layers.

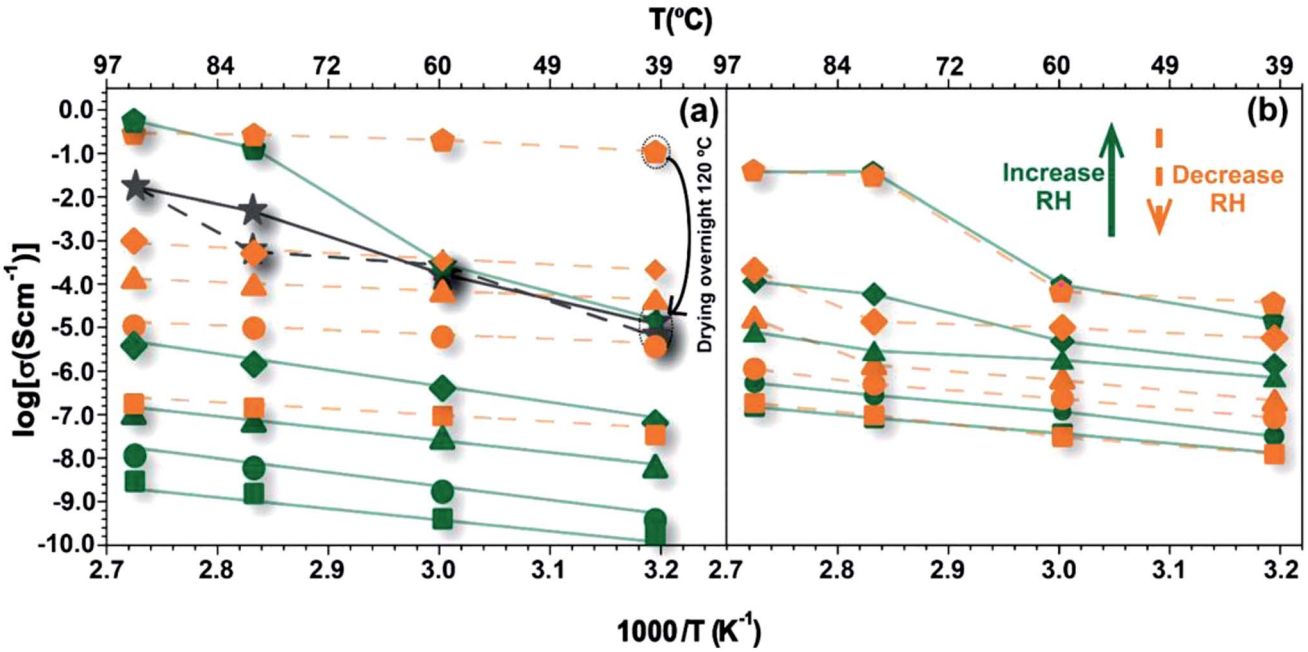

Fig. 3 Arrhenius plots for the proton conductivity of pristine samples of (a) $[Gd(H_4nmp)(H_2O)_2]Cl\cdot 2H_2O$ (**1**) and (b) $[Gd_2(H_3nmp)_2]\cdot xH_2O$ (**2**) ($x = 1$ to 4) measured at variable RH values (⬟ – 98%, ◆ – 80%, ▲ – 60%, ● – 40%, and ■ – 20%), with the 1st run data in green, 2nd run data in orange and 3rd run in black.

led to the concomitant release of hydrochloric acid (evidenced also by corrosion of stainless steel ancillaries of the conductivity jig, in the sample vicinity, and the absence of chloride ions in the final sample as observed in Fig. S11†). This process consumes water and one can expect an irreversible and larger water uptake for **1** than for **2**, as confirmed experimentally from the water vapour sorption isotherms (see the next section for further details).

The increase of temperature and release of the chloride anion induce changes in the metallic coordination environment; several covalent Gd–O bonds are destroyed or rearranged (from the phosphonate groups, Fig. S5 in the ESI†) and all coordination water molecules are removed. The newly formed covalent connections induce the formation of a more compact $^{2}_{\infty}[Gd_2(H_3nmp)_2]$ neutral layer as present in the structural model of **2sc**, with the transformation being similar to the folding of a sheet of paper (see Fig. S6, in the ESI,† for a topological perspective of this structural transformation).

This swelling of the material occurs naturally and over time, being mostly an effect driven by kinetic features. Fig. S3 (in the ESI)† shows that over a period of 8 months a representative sample of **2** captures water molecules from air, with the concomitant swelling being observed by the shifting of the (002) reflection to lower 2 theta angles. This evidence supports not only the aforementioned transformation process of **1** into **2**, but also the variable water content observed for the various prepared compounds.

Proton conductivity

The temperature dependence of ionic conductivity at different RH values for **1** is depicted in Fig. 3a. As presented in Fig. S1,† the synthetic method does not change the crystalline phase of the material. For this reason, the following studies were conducted on the CPs obtained by the one-pot synthesis (**1op** and **2op**). The conductivity measurements were firstly carried out with increasing temperature (1st run), at each RH value, and then during cooling down (2nd run). As usually observed for water-mediated protonic conductors, conductivity increases with RH, although for temperatures higher than 60 °C at 98% RH this increase is especially noticeable. The conductivity at 94 °C and 98% RH reaches a maximum of 0.51 S cm^{-1}, which represents an increment of about 5 orders of magnitude with respect to measurements at 80% RH. The value is amongst the highest conductivity values reported for a proton-conducting MOF material,[13,23–26] being comparable, or even higher, than data typically found for Nafion.[27,28] Top conductivity values reported for MOFs are found to be around 0.15 S cm^{-1} at 80 °C and 98% RH, obtained for proton-conducting coordination polymers with frameworks neutralized by different templated polycarboxylate anions[25] or, more recently, for a MOF-based composite reported by Li *et al.* which exhibits a conductivity of 1.82 S cm^{-1} at 70 °C and 90% RH.[29] At this point it is important to underlie the conductivity results reported by Bazaga-García *et al.*[19] for Gd–H_4NMPCl, which is essentially **1**. Their data obtained at 40 °C and 95% RH ($\sim 3.5 \times 10^{-5}$ S cm^{-1}) agree remarkably well with our own data collected at the same temperature and 98% RH ($\sim 1.5 \times 10^{-5}$ S cm^{-1}), considering that the measurements are conducted on compacted powders and using different experimental set-ups (namely the electrodes, which are made of carbon in their case and of silver in ours). Large differences, however, become apparent when increasing the temperature at high RH, where Gd–H_4NMPCl

reported by Bazaga-García *et al.* shows a proton conductivity of 3×10^{-4} S cm^{-1} at 80 °C and 95% RH, a considerably lower value when compared with ours for **1** (0.1 S cm^{-1} at 80 °C and 98% RH). The data for **1** at 98% RH (Fig. 3a) deviate from the linear Arrhenius tendency depicting a distinct Z-shape with a step increase between 60 °C and 80 °C, indicating a change to a transport mechanism enabling much higher conductivities (see Section 4 in the ESI† for further details). Interestingly, the data from Bazaga-García *et al.* also show this characteristic transition at around 60 °C, although attaining lower conductivity than in our case. The authors did not consider this transition and fitted the data to the Arrhenius model with an average activation energy of 47.3 kJ mol^{-1}.[18]

On resuming the analysis of our data, one notes that **1** also shows Arrhenius behaviour with activation energies varying from 53 kJ mol^{-1} to 76 kJ mol^{-1} with increasing RH from 20% to 80%. Such apparent increase in the activation energy can actually be a hint of the phase transition occurring at progressively lower temperatures with increasing RH, which becomes explicit only at 98% RH in the temperature range covered in our study. As detailed in the previous section, this transition observed at *ca.* 60 °C and 98% RH is linked to exchange of Cl$^-$ anions of the sample for absorbed water molecules. This has been further confirmed by the observation of oxidized stainless steel screws and nuts from the sample holder, which is compatible with the formation of HCl resulting from the ionic exchange. Also, powder X-ray diffraction (change into a phase without Cl$^-$ in the structure) and EDS analysis of several crystals show the absence of Cl$^-$ in the structure (Fig. S11†). The detailed study of the ionic exchange mechanism is out of the scope of this paper, but we assume that this must necessarily start on the surface of the particles, and from there proceed inside the crystal involving diffusion of Cl$^-$ anions from the bulk to the surface driven by the inclusion of water molecules. This surface process generates an additional impedance that correlates with the low frequency contribution in the spectra shown in Fig. S7.† This impedance is significantly reduced at high temperatures and high humidity (Fig. S7b *versus* S7c†) and it is not observed in the spectra collected in the second run of **1**, nor in the spectra of the Cl-free compound **2** (Fig. S8†).

The conductivity values of **1** collected at 98% RH with decreasing temperature (2nd run) are still in the range of 0.3–0.1 S cm^{-1}, but at 40 °C and 40% RH the conductivity is four orders of magnitude higher than that measured in the 1st run. The large difference in conductivity, and in the activation energy (E_a), between the 1st and 2nd runs (Table S5†) suggests different mechanisms to explain the conduction process of **1**. In the 1st run, E_a was found to be much higher than that of typical hydrated protonic conductors, such as Nafion (E_a = 21 kJ mol^{-1}),[30] increasing with RH, particularly near saturation. This suggests that the additional energy associated with the conduction process in **1** may be related to processes involving the exchange of Cl$^-$ anions. Other water-mediated proton-conducting MOFs reported in the literature[31–34] also have high E_a values, usually in the range 55–130 kJ mol^{-1}, which were attributed to non-efficient proton transfer pathways,[32] direct diffusion of additional protons with water molecules or the presence of other guest molecules[34] and small apertures between the micropores.[31,33] The temperature dependence of conductivity for the 2nd run displays a typical linear Arrhenius trend, with activation energy in the range 20–32 kJ mol^{-1}. The lower E_a values indicate that charge transport mainly occurs through structural diffusion, which seems to be the result of a wider and more efficient proton-conducting pathway. The 3rd run of measurements (carried out after drying the transformed **1** at 120 °C) further shows that the extraordinarily high conductivity at a low temperature, paired with the apparent linear Arrhenius dependence evidenced by the data measured in the 2nd run of **1** at 98% RH, is likely to be due to a transient effect of water and chlorine ions retained in the structure after the 1st run of measurements (note that the pellet remains at 98% RH between the two measurements), which is effectively removed from the structure only after the high temperature intermediate drying step. One may note that the 3rd run curve (seen in black in Fig. 3a) starts at the same conductivity level of the pristine pellet, which suggests that the structural modification underlying the abrupt conductivity increase with temperature at 98% RH occurs predominantly on the final chlorine-free material. The analysis of the structural transformation underlying the conductivity enhancement between 60 °C and 80 °C is thus fundamental to understand and explain the high conductivity values of this material.

The X-ray patterns displayed in Fig. S9 in the ESI† indicate an unequivocal structural transformation of **1** into **2** above 80 °C under nearly saturated conditions, which could explain the abrupt increase of conductivity in the 1st run. Because this occurs in the pelleted form of the material, we assume that this structural transformation is mostly based on a typical single-crystal to single-crystal (SC–SC) transformation in which crystallites of **1** convert into $[Gd_2(H_3nmp)_2]\cdot xH_2O$ (**2**) ($x = 1$ to 4) (see the previous section for further details on the transformation process). We remind that **2** has neutral layers interconnected by hydrogen bonding contacts involving phosphonate groups and crystallization water molecules. Apparently, the change in conductivity may be attributed to the transformation of the hydrogen bonding network induced by humidity and high temperatures, which contributes to the release of the chloride anions in the form of HCl. Powder X-ray diffraction of the pellet after conductivity measurements confirms the presence of **2** (Fig. S10 in the ESI†). These studies demonstrate that after the release of chloride anions the interlayer spacing increases by about 3 Å, allowing the transport of a higher number of protons. Also, all coordination water molecules were removed and the layers of **2** stack on top of each other, being maintained by hydrogen interactions with the remaining crystallization water molecules. Though these interactions are of variable strength [$d_{O\cdots H}$ = 2.53(5)–3.30(4) Å] and directionality [$\angle$(OHO) = 119–175°], they nevertheless allow a fast proton transfer between neighbouring phosphonate groups and water molecules which the material can readily adsorb when exposed to a humid atmosphere (see water vapour sorption isotherms in Fig. S12†). The bulk structure transformation also induced a chemical modification of the framework, providing an increase in free acidic protons from the partially protonated ligand.[24] Contrary

to **1**, given the synthetic conditions of **2** one may expect this compound to resist moderately high temperatures and humidity conditions found in applications such as fuel cells.

There is thus an obvious interest in studying the conductivity of **2**. These data are shown in Fig. 3b, where the similar conductivity collected during heating and cooling denotes no transformation between the first and second run of measurements of **2**. It should be noted that some variations in the sample resistance are expected due to structural rearrangements leading to changes in particle connectivity following the interaction with water. Considering these limitations of powder compacts, the remarkable agreement of both sets of data supports the assumption that **1** transforms into **2** under wet conditions, in full agreement with Fig. S10.† In fact, such small differences in conductivity when the sample is submitted to various thermal and humidity cycles support the supposed chemical stability of **2** at high temperatures and under high humidity conditions.

As observed in the 3rd run data for **1**, the conductivity of **2** at 98% depicts a sharp increase at around 60 °C which is likely due to a structural transition induced by temperature only at high humidity levels, when the interlayer space of **2** is filled with water. Note that the presence of water is key to enable this transition, as all sets of conductivity data collected at 80% RH or lower humidity display the linear Arrhenius dependence. One may thus assume that the adsorbed interlayer water weakens the hydrogen bonds which, by the effect of temperature, changes their structure enabling enhanced proton mobility and conductivity (one may note that the conductivity measurements are made at constant RH, and the water content is kept constant at any given temperature). The underlying structural change is probably related to subtle rearrangements of the hydrophilic domains formed by the phosphonate groups and the water molecules, which are difficult to characterize by conventional diffraction techniques. Indeed, PXRD patterns collected at constant 95% RH at 25 °C and 80 °C are practically identical (Fig. S13†), which confirms that the structural differences underlying the conductivity enhancement are indeed subtle but sufficient to boost proton mobility (and thus the conductivity) along the interlayer space of **2**. The fact that the activation energy for the conductivity of **2** is close to 30 kJ mol^{-1}, which is similar to that observed for the second run of **1** (Table S5†), reinforces the idea that the proton transport along the interlayer space in **2** occurs predominantly through a facile structural diffusion. While under these conditions the framework of **2** should play an active role in the proton structural diffusion by assisting proton hopping, one cannot rule out the contribution of molecular diffusion of water molecules along the channels for low hydration levels. Further work is necessary to elucidate the details of the proton transport mechanism in these materials, namely the structural study of **2** by neutron diffraction and solid-state NMR at variable temperature and relative humidity. A deeper knowledge of the structure makes it possible to design molecular dynamics and DFT atomistic simulations to gain the desired insight into the structure/proton conductivity relationship of these highly conducting materials. Such studies may also provide valuable information about the stability of **2** at high temperature and under high humidity conditions.

Conclusions and outlook

We report the transformation of $[Gd(H_4nmp)(H_2O)_2]Cl\cdot 2H_2O$ (**1**) into $[Gd_2(H_3nmp)_2]\cdot xH_2O$ (**2**) at high temperatures and relative humidity (RH) and its remarkable effect on proton conductivity. While **1** presents conductivity values reaching 1.23×10^{-5} S cm^{-1} at near ambient temperature and RH, an increase in conductivity is especially observed between 80 and 98% RH, reaching a value of 0.51 S cm^{-1} (increment of 5 orders of magnitude), representing one of the highest conductivity values reported for a proton-conducting MOF. This significant increase is observed during *in situ* transformation of **1** into **2**. On the other hand, we show that **2** can easily be prepared as a pure-phase material by three sustainable methods (conventional hydrothermal, microwave-assisted and one-pot conditions), showing conductivity values in the region of 3.79×10^{-2} S cm^{-1} at 94 °C and 98% RH, ranking this material as one of the best conducting MOFs reported so far. This difference in conductivity between the as-synthesized **2** and **1** after transformation led us to conclude that the high value of 0.51 S cm^{-1} must be related to a high number of charge carriers from the solvation of chloride anions by the water molecules that are present in the material when it is still inside the climatic chamber. During transformation, a large number of water molecules are adsorbed (the water adsorption isotherms of the two compounds show that **1** is more hydrophilic than **2**, with 23% increased mass at 98% RH), and they are permuted with the chloride anions and stacked in-between the layers. This allied with layer rearrangement, the formation of new hydrogen bonding interactions and the rich acidic medium in the climatic chamber leads to this increase in conductivity. In truth, when the pellet of **1**, after transformation, is dried at 120 °C the conductivity values are in the same range as those obtained for as-synthesized **2**.

The highest conductivity value obtained for **1** after being transformed (especially if we maintain the high humidity environment) and even the high conductivity of **2**, are unequivocal evidence that phosphonate-based materials (particularly hydrophilic layered materials) can have great potential for this kind of application. The present report arises as an interesting "proof of concept" that will allow us in the future to better design and prepare new materials where this "anionic exchange" can be either controlled *via* a process with slower kinetics or modified to a new one that can be reversible so as to explore the remarkable proton conductivity of these materials.

Conflicts of interest

There are no conflicts to declare.

Acknowledgements

We wish to thank Fundação para a Ciência e a Tecnologia (FCT, Portugal), the European Union, QREN, FEDER through

Programa Operacional Factores de Competitividade (COMPETE), UniRCell (SAICTPAC/0032/2015 and POCI-01-0145-FEDER-016422) and CICECO-Aveiro Institute of Materials (FCT Ref. UIDB/50011/2020 & UIDP/50011/2020), financed by national funds through the FCT/MEC and appropriately co-financed by FEDER under the PT2020 Partnership Agreement. FCT is also gratefully acknowledged for the PhD grant no. SFRH/BD/46601/2008 (to PS), and the Development grant no. IF/01174/2013 (to FF). RFM also gratefully acknowledges FCT for the Junior Research Position (CEECIND/00553/2017).

References

1 M. Eddaoudi, D. F. Sava, J. F. Eubank, K. Adil and V. Guillerm, *Chem. Soc. Rev.*, 2015, **44**, 228–249.
2 M. J. Zaworotko, *Nature*, 2008, **451**, 410–411.
3 Y. B. He, W. Zhou, G. D. Qian and B. L. Chen, *Chem. Soc. Rev.*, 2014, **43**, 5657–5678.
4 R. F. Mendes, M. M. Antunes, P. Silva, P. Barbosa, F. Figueiredo, A. Linden, J. Rocha, A. A. Valente and F. A. A. Paz, *Chem.–Eur. J.*, 2016, **22**, 13136–13146.
5 A. H. Chughtai, N. Ahmad, H. A. Younus, A. Laypkov and F. Verpoort, *Chem. Soc. Rev.*, 2015, **44**, 6804–6849.
6 K. C. Stylianou, R. Heck, S. Y. Chong, J. Bacsa, J. T. A. Jones, Y. Z. Khimyak, D. Bradshaw and M. J. Rosseinsky, *J. Am. Chem. Soc.*, 2010, **132**, 4119–4130.
7 J. Zhang, B. Zheng, T. T. Zhao, G. H. Li, Q. S. Huo and Y. L. Liu, *Cryst. Growth Des.*, 2014, **14**, 2394–2400.
8 J. Della Rocca, D. M. Liu and W. B. Lin, *Acc. Chem. Res.*, 2011, **44**, 957–968.
9 P. Horcajada, R. Gref, T. Baati, P. K. Allan, G. Maurin, P. Couvreur, G. Ferey, R. E. Morris and C. Serre, *Chem. Rev.*, 2012, **112**, 1232–1268.
10 A. U. Czaja, N. Trukhan and U. Müller, *Chem. Soc. Rev.*, 2009, **38**, 1284–1293.
11 P. Silva, S. M. F. Vilela, J. P. C. Tomé and F. A. A. Paz, *Chem. Soc. Rev.*, 2015, **44**, 6774–6803.
12 B. Yilmaz, N. Trukhan and U. Müller, *Chin. J. Catal.*, 2012, **33**, 3–10.
13 P. Ramaswamy, N. E. Wong and G. K. H. Shimizu, *Chem. Soc. Rev.*, 2014, **43**, 5913–5932.
14 G. K. H. Shimizu, J. M. Taylor and K. W. Dawson, in *Metal Phosphonate Chemistry: From Synthesis to Applications*, The Royal Society of Chemistry, 2012, pp. 493–524.
15 S. Bi, H. Banda, M. Chen, L. Niu, M. Chen, T. Wu, J. Wang, R. Wang, J. Feng, T. Chen, M. Dincă, A. A. Kornyshev and G. Feng, *Nat. Mater.*, 2020, **19**, 552–558.
16 J. Cao, W. Ma, K. Lyu, L. Zhuang, H. Cong and H. Deng, *Chem. Sci.*, 2020, **11**, 3978–3985.
17 D. A. Levenson, J. Zhang, P. M. J. Szell, D. L. Bryce, B. S. Gelfand, R. P. S. Huynh, N. D. Fylstra and G. K. H. Shimizu, *Chem. Mater.*, 2020, **32**, 679–687.
18 D. Bradshaw, A. Garai and J. Huo, *Chem. Soc. Rev.*, 2012, **41**, 2344–2381.
19 M. Bazaga-García, G. K. Angeli, K. E. Papathanasiou, I. R. Salcedo, P. Olivera-Pastor, E. R. Losilla, D. Choquesillo-Lazarte, G. B. Hix, A. Cabeza and K. D. Demadis, *Inorg. Chem.*, 2016, **55**, 7414–7424.
20 S. Begum, Z. Y. Wang, A. Donnadio, F. Costantino, M. Casciola, R. Valiullin, C. Chmelik, M. Bertmer, J. Karger, J. Haase and H. Krautscheid, *Chem.–Eur. J.*, 2014, **20**, 8862–8866.
21 M. Yoon, K. Suh, S. Natarajan and K. Kim, *Angew. Chem., Int. Ed.*, 2013, **52**, 2688–2700.
22 *Metal Phosphonate Chemistry: From Synthesis to Applications* ed., A. Clearfield and K. Demadis, Royal Society of Chemistry, 2012.
23 W. J. Phang, H. Jo, W. R. Lee, J. H. Song, K. Yoo, B. Kim and C. S. Hong, *Angew. Chem., Int. Ed.*, 2015, **54**, 5142–5146.
24 M. Sadakiyo, T. Yamada and H. Kitagawa, *ChemPlusChem*, 2016, **81**, 691–701.
25 S. M. Elahi, S. Chand, W. H. Deng, A. Pal and M. C. Das, *Angew. Chem., Int. Ed.*, 2018, **57**, 6662–6666.
26 F. Yang, G. Xu, Y. B. Dou, B. Wang, H. Zhang, H. Wu, W. Zhou, J. R. Li and B. L. Chen, *Nat. Energy*, 2017, **2**, 877–883.
27 N. C. Rosero-Navarro, E. M. Domingues, N. Sousa, P. Ferreira and F. M. L. Figueiredo, *Solid State Ionics*, 2014, **262**, 324–327.
28 R. Yadav and P. S. Fedkiw, *J. Electrochem. Soc.*, 2012, **159**, B340–B346.
29 X. M. Li, L. Z. Dong, S. L. Li, G. Xu, J. Liu, F. M. Zhang, L. S. Lu and Y. Q. Lan, *ACS Energy Lett.*, 2017, **2**, 2313–2318.
30 K. D. Kreuer, S. J. Paddison, E. Spohr and M. Schuster, *Chem. Rev.*, 2004, **104**, 4637–4678.
31 P. Barbosa, N. C. Rosero-Navarro, F. N. Shi and F. M. L. Figueiredo, *Electrochim. Acta*, 2015, **153**, 19–27.
32 X. Meng, S. Y. Song, X. Z. Song, M. Zhu, S. N. Zhao, L. L. Wu and H. J. Zhang, *Chem. Commun.*, 2015, **51**, 8150–8152.
33 M. Sadakiyo, H. Kasai, K. Kato, M. Takata and M. Yamauchi, *J. Am. Chem. Soc.*, 2014, **136**, 1702–1705.
34 M. Sadakiyo, T. Yamada and H. Kitagawa, *J. Am. Chem. Soc.*, 2009, **131**, 9906–9907.